Heliyon 9 (2023) e13094

Contents lists available at ScienceDirect

Heliyon

journal homepage: www.cell.com/heliyon

Research article

Automatic treatment outcome prediction with DeepInteg based on multimodal radiological images in rectal cancer

Yihuang Hu [a,1], Juan Li [b,1], Zhuokai Zhuang [c,d,1], Bin Xu [a,1], Dabiao Wang [e,*], Huichuan Yu [f,**], Lanlan Li [a,***]

[a] Fujian Key Lab for Intelligent Processing and Wireless Transmission of Media Information, College of Physics and Information Engineering, Fuzhou University, Fuzhou, 350108, China
[b] Department of Endoscopic Surgery, The Sixth Affiliated Hospital, Sun Yat-sen University, Guangzhou, Guangdong, 510655, China
[c] Guangdong Institute of Gastroenterology, Guangdong Provincial Key Laboratory of Colorectal and Pelvic Floor Disease, The Sixth Affiliated Hospital, Sun Yat-sen University, Guangzhou, Guangdong, 510655, China
[d] Department of Colorectal Surgery, The Sixth Affiliated Hospital, Sun Yat-sen University, Guangzhou, Guangdong, 510655, China
[e] College of Chemical and Engineering, Fuzhou University, Fuzhou, 350108, China
[f] Guangdong Institute of Gastroenterology, Guangdong Provincial Key Laboratory of Colorectal and Pelvic Floor Disease, The Sixth Affiliated Hospital, Sun Yat-sen University, 26 Yuancun Erheng Road, Guangzhou, Guangdong, 510655, China

ARTICLE INFO

Keywords:
Deep learning
MRI
CT
Neoadjuvant therapy
Rectal cancer

ABSTRACT

Neoadjuvant systemic treatment before surgery is a prevalent regimen in the patients with advanced-stage or high-risk tumor, which has shaped the treatment strategies and cancer survival in the past decades. However, some patients present with poor response to the neoadjuvant treatment. Therefore, it is of great significance to develop tools to help distinguish the patients that could achieve pathological complete response before surgery to avoid inappropriate treatment. Here, this study demonstrated a multi-task deep learning tool called DeepInteg. In the DeepInteg framework, the segmentation module was constructed based on the CE-Net with a context extractor to achieve end-to-end delineation of region of interest (ROI) from radiological images, then the features of segmented Magnetic Resonance Imaging (MRI) and Computed Tomography (CT) images of each case were fused and input to the classification module based on a convolution neural network for treatment outcome prediction. The dataset with 1700 MRI and CT slices collected from the prospectively randomized clinical trial (NCT01211210) on systemic treatment for rectal cancer was used to develop and systematically optimize DeepInteg. As a result, DeepInteg achieved automatic segmentation of tumoral ROI with Dices of 0.766 and 0.719 and mIoUs of 0.788 and 0.756 in CT and MRI images, respectively. In addition, DeepInteg achieved AUC of 0.833, accuracy of 0.826 and specificity of 0.856 in the prediction for pathological complete response after treatment, which showed better performance compared with the model based on CT or MRI alone. This study provide a robust framework to develop disease-specific tools for automatic delineation of ROI and clinical outcome prediction. The well-trained DeepInteg could be readily applied in clinic to predict pathological complete response after neoadjuvant therapy in rectal cancer patients.

* Corresponding author.
** Corresponding author.
*** Corresponding author.
E-mail addresses: wangdb19@fzu.edu.cn (D. Wang), yuhch5@mail.sysu.edu.cn (H. Yu), lilanlanfzu@outlook.com (L. Li).
[1] Contribute equally to this work.

https://doi.org/10.1016/j.heliyon.2023.e13094
Received 23 July 2022; Received in revised form 4 January 2023; Accepted 16 January 2023
Available online 25 January 2023

1. Background

Neoadjuvant therapy is a widely used regimen prior to surgical treatment for multiple solid tumors with advanced clinical stages or high-risk features [1–3]. It may enable patients to avoid inappropriate treatment and obtain effective therapy by evaluating whether patients could achieve good response before the treatment [4–7]. Among these patients, those achieving pathological complete response (pCR) without residual cancer cells and receiving "organ preservation" procedures can benefit from less surgical complications and improved quality of life after the systemic treatment [6,8,9].

However, pathological response can only be confirmed by examining the samples removed after surgery. Therefore, multiple studies have been conducted previously to develop reliable non-invasive methods to assist the evaluation of pathological response in the systemic cancer treatment [10–12]. Reachers also showed the potential of the multimodal models based on clinicopathological and radiomic features in predicting pathological response to cancer treatment by using machine learning approaches in previous studies [13–15]. In recent years, deep learning has shown promising value in image analysis to assist the clinical decision on cancer or other treatment [16–19]. Currently, deep learning-based tools have been developed for diagnosis of disease status in the serial management of patients by using multiple types of medical image [20–23].

This study aimed to develop an end-to-end model called DeepInteg for automatic segmentation and outcome prediction by fusing MRI and CT images to predict pCR in a prospectively randomized controlled trial. DeepInteg is an applicable deep learning-based framework for treatment outcome prediction that can be used in the provided data set. We expect that DeepInteg can assist the current judgement on image-based clinical complete response to guide cancer treatment decisions and the design of imaging marker-driven clinical trials.

The rest of this paper is organized as follows: Materials and methods introduced the data sources and the structure of the model. The chapter of Results compared the performance of different modal models and selects the best model. In the discussion section, we discussed the applicability of DeepInteg and the direction for improvement. We concluded this study in the last chapter.

2. Materials and methods

2.1. Patient dataset

The dataset used for training and validation of DeepInteg came from the FOWARC (NCT01211210) trial led by the Sixth Affiliated Hospital of Sun Yat-sen University. The FOWARC trial included patients with locally advanced rectal cancer (cT3-4 and/or cN1-2, stage c II -III), as we previously described [24,25]. All patients underwent radical surgery 6–8 weeks after neoadjuvant therapy and the resected specimens were evaluated by pathologists for treatment response assessment. A total of 99 patients with 850 imaging slices of portal venous-phase contrast-enhanced CT and 850 T^2-weighted MRI slices before treatment were included in this study. The patients were randomly assigned to the training and validation set according to the proportion of 2:1 cases.

The clinical and demographic characteristics along with the imaging profiles of the study patients were obtained from the FOWARC trial working group and the collaborating team of Institutional Database Program of Colorectal Disease of Sixth Affiliated Hospital of Sun Yat-sen University [26–28]. The pathological response after neoadjuvant treatment was evaluated by two experienced pathologists using the tumor response grading (TRG) system [29]. The patients were divided into two groups: pCR group (TRG0, no visible residual tumor cells) and non-pCR group (TRG1∼4, ranging from rare residual cancer cells to extensive residual cancer cells).

All patients received CT and MRI scans within one week before the neoadjuvant treatment. The imaging data was retrieved from the picture archiving and communication system (PACS, Carestream, Canada). The marked region of interest (ROI) covering tumors was delineated by two experienced radiologists using itk-SNAP software (version 3.8.0, www.itksnap.org). Both radiologists were blind to the clinicopathological information of each patient. The MRI and CT images were preprocessed as two-dimensional images and normalized to a size of $512 \times 512 \times 3$. To reduce the possible impact of brightness on model performance, The images were then preprocessed with a Laplacian of Gaussian (LoG) filter to remove noise and enhance texture features [30]. The difference of images before and after preprocessing was shown in Fig.S1 (Supplementary Material).

2.2. Framework of DeepInteg

We proposed a model for predicting pCR based on an end-to-end procedure including the segmentation module and the classification module. The segmentation module of DeepInteg was constructed based on CE-Net [31], which was trained to automatically delineate tumoral region of interest (ROI). In addition, the context extractor of the network can extract deeper image features and avoid the loss of some spatial information. Then the binary mask obtained by segmentation was used to locate and crop the tumor region and para-cancerous area to generate a square ROI, which was restored to images of different sizes by interpolation and used for prediction of the pCR probability through the integrated voting of pictures by the convolutional neural network. In general, the ResNet block pre-trained on ImageNet was used in the feature encoder in the segmentation part, which added a context extractor to capture more high-dimensional features and retain more spatial information. In the outcome classification step, the multimodal images were fused, then they were used for outcome prediction. The overall workflow of this study was shown in Fig. 1.

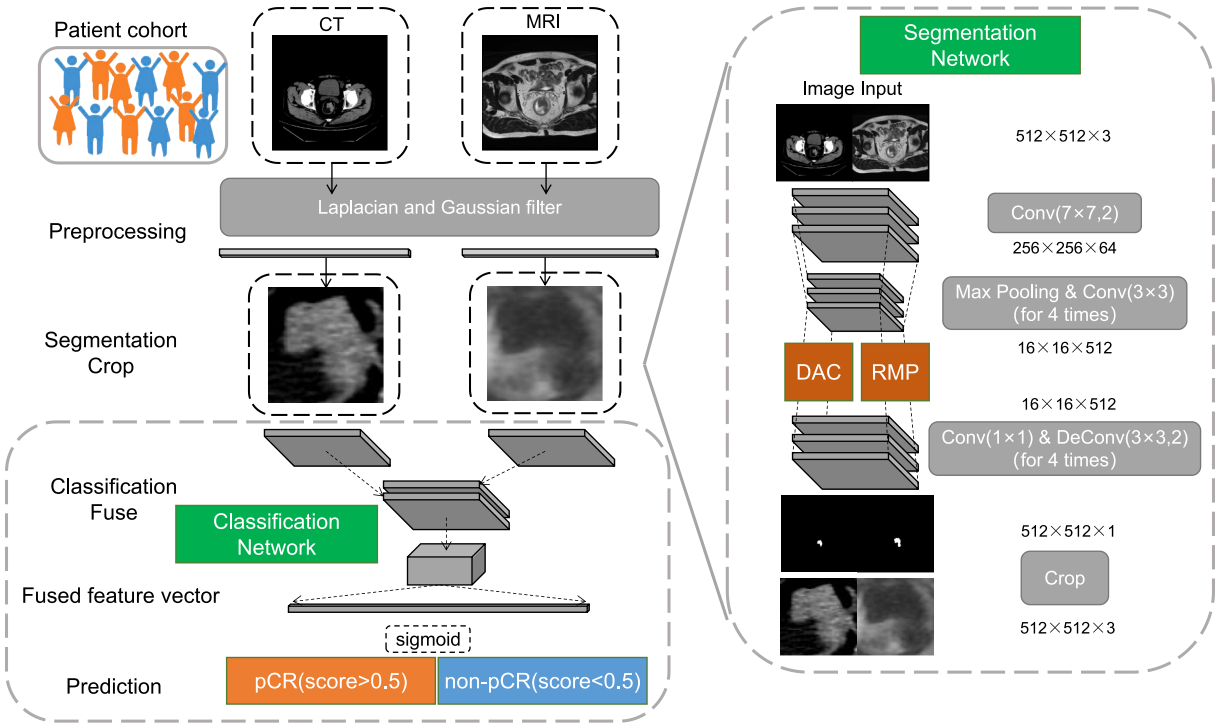

Fig. 1. The Overall workflow of DeepInteg. DeepInteg contained two modules: the segmentation module and the classification module. The segmentation module was based on CE-Netwhich could obtain deeper image features by the context extractor to avoid loss spatial information. The segmented binary mask was then located to the image to crop the square tumor region. After restoring the cropped image to different sizes the classification module could predict, the probability of pCR for the patient by a dual-channel convolution neural network.

2.3. Segmentation

Many reported deep learning-based segmentation may cause the loss of useful information due to frequent convolution and pooling, resulting in inaccurate segmentation. To solve these problems, we used CE-Net [31] for tumor segmentation that added a context extractor based on the U-Net [32] and adjusted some convolution and encoding and decoding methods. The structure of CE-Net network was shown in Fig. S2 (Supplementary Material).

2.4. Classification

The image fusion by conventional methods, which included feature addition and superposition, could make full use of the unique feature information of MRI and CT. As the features of MRI and CT images were different, feature addition may lead to confusion, which degraded the performance of classification network. Therefore, feature superposition was more reasonable to enrich the features of images and improve the classification network. To establish the pCR prediction model, we used convolutional neural network for image fusion feature extraction and classification on cropped CT and MRI images. Our classification model mainly contained two types of layers, including the convolutional layer for extracting information from imaging features and a fully connected layer for mapping between convolutional features and pCR.

3. Result

3.1. Optimization of accurate segmentation for tumoral ROI

The comparison of segmentation performance between U-Net and CE-Net was shown in Fig. 2. The U-Net may misclassify some tumor pixels as non-tumor pixels, which would reduce the accuracy of segmentation. The CE-Net had the function of context extraction, which could learn to extract richer feature information, and promote tumor boundary prediction. Table 1 showed the detailed segmentation performance of U-Net and CE-Net in MRI and CT. The CE-Net performed better in the accuracy, sensitivity and specificity in predicting the lesion area. In addition, the CE-Net segmentation had higher Dice and mIoU in predicting the shape of the lesion area in CT (0.766 and 0.719) and MRI images (0.788 and 0.756), respectively. Therefore, we applied the CE-Net in the segmentation network of DeepInteg.

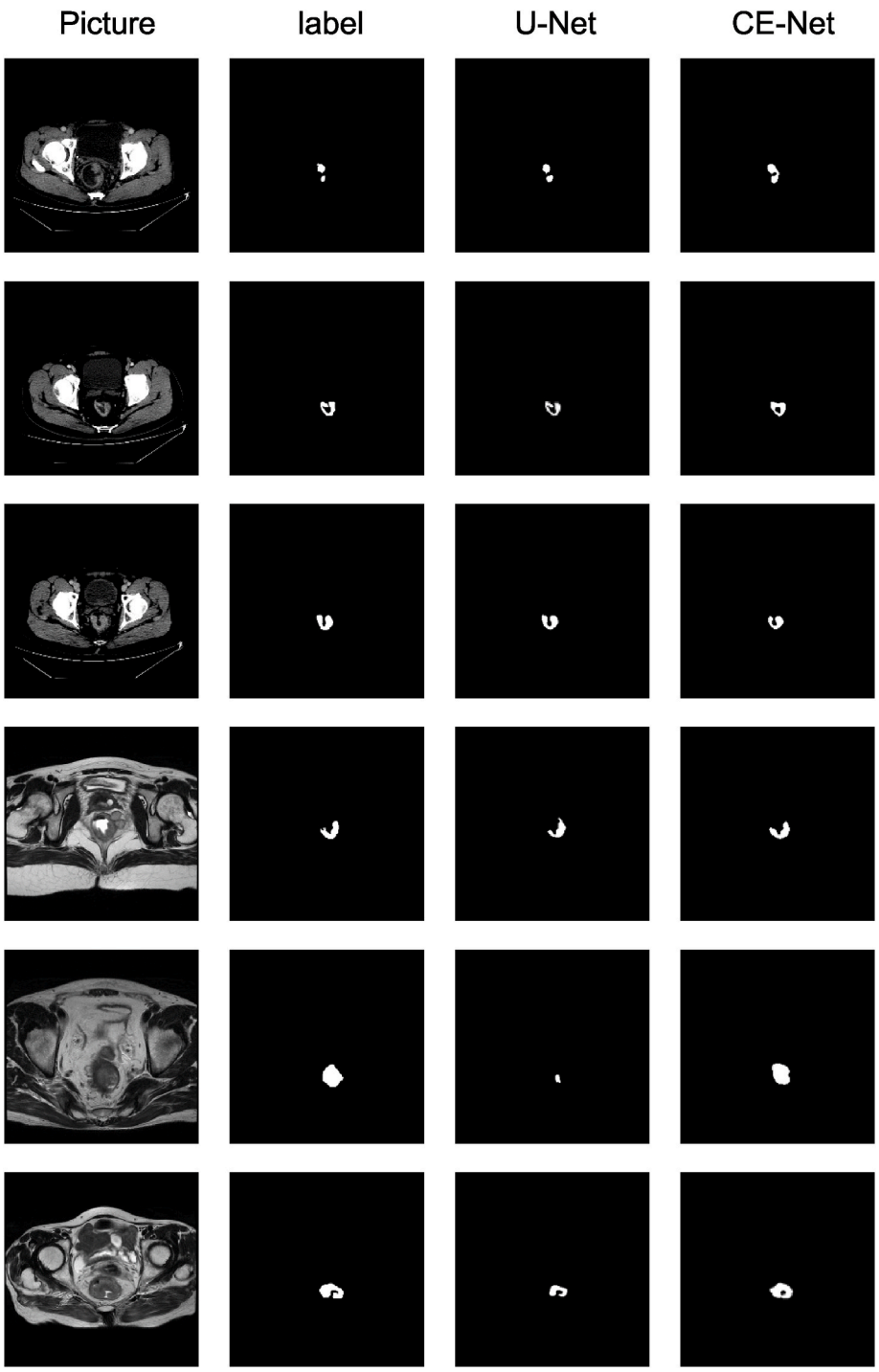

Fig. 2. Performance of partial segmentation by models based on U-Net and CE-Net. The size of the original image was 512 × 512 × 3 and the size of the label and prediction image was 512 × 512 × 1.

3.2. Treatment outcome prediction with DeepInteg

In this study, the classification model was constructed based on the convolution voting procedure which considered tumor regions from both CT and MRI images to avoid misjudgment caused by insufficient features from single image modality. These regions were automatically cropped by the segmentation module as described above. To compare the impact of image sizes on classification, we preprocessed the picture by interpolation, converted them to three different sizes (64 × 64, 128 × 128, and 256 × 256) and trained

Table 1
Segmentation performance of U-Net and CE-Net in the validation set of patient MRI and CT images.

Net	Type	*accuracy*	*sensitivity*	*specificity*	*Dice*	*mIoU*
U-Net[21]	CT	0.887	0.833	0.922	0.731	0.687
	MRI	0.862	0.780	0.910	0.785	0.754
CE-Net[20]	CT	0.925	0.874	0.960	0.766	0.719
	MRI	0.914	0.812	0.988	0.788	0.756

models based on these images respectively. In order to verify that MRI and CT fusion can have better performance, we divided the experiments into three models: CT model, MRI model, and CT and MRI fusion model for comparison and verification.

The comparison of classification performance of models based on different images sizes was shown in Fig. 3A. In the CT-based models, the classification model for images of size 128 × 128 achieved the highest AUC of 0.780 (95%CI: 0.602–0.905). In the MRI-based models, the classification model for images of size 256 × 256 achieved the highest AUC of 0.801 (95%CI: 0.623–0.921). In the models integrating both CT and MRI, the highest AUC was 0.833 (95%CI: 0.660–0.941) for the classification model with images of size 256 × 256. We also compared the classification performance of models based on CT and MRI fused images. As shown in Fig. 3. (A-D), the classification performance of the network was improved as the channel fusion increased the number of effective features of the network. The classification model based on fusion of CT and MRI images achieved the highest AUC of 0.833 (95%CI: 0.660–0.941), accuracy of 0.826 (95%CI: 0.713–0.894) and specificity of 0.856 (95%CI: 0.748–0.943) compared to CT- or MRI-based models.

4. Discussion

In this study, we established a deep learning model named “DeepInteg” that integrated tumor segmentation and pCR classification based on multimodal images, which provided an end-to-end tool for clinicians to automatically delineate tumor regions and determined whether LARC patients could achieve pCR after neoadjuvant treatment. In the DeepInteg, we fused the image features of MRI and CT, as they reflect the characteristics of tumors from different modalities [33]. DeepInteg can be easily accessed and applied to the clinical settings with other cancer patients undergoing neoadjuvant treatment before surgery to predict the disease status in the serial management.

We used four-fold triple cross-validation to evaluate the performance of the model and chose CE-Net with context extractor for segmentation network, as it had high adaptability in the segmentation of image details and the complexity of image texture. The context extractor can better grasp the texture of images and the details of the tumor. In the classification part, preliminary experiments found that the classification effect was better in 4 convolutional layers. The extracted feature information was not sufficient when the number of convolutional layers was relatively lacking, while larger number of layers may lead to over-detailed features and learn tumor features unreasonably. For the calculation of the probability in the classification model, Fu et al. [34] directly extracted images corresponding to the largest tumor area of each patient to predict pCR, while Kim et al. [35] took the average of the patient’s multi-frame images to perform prediction on the patient classification. For a comprehensive and effective judgment on achieving pCR, and avoid interference, we used different frames of images from each patient to integrate voting to obtain the probability of pCR.

Our fusion model achieved an AUC of 0.833, which was higher than models using CT or MRI alone. Among different image sizes, the AUC of the classification model with images of size 256 × 256 was higher than models based on the other two sizes of images. Therefore, the 256 × 256 image should be chosen as the input for the classification module. MRI and CT contained different tumor information features, and the effective use of tumor features from two different images were important for performance improvement. In this study, the channel fusion method was used in the convolution layer to fuse the two image features, which increased the number of features and improved the performance to a certain extent.

However, our study still had certain limitations. First, sample size of our study is relatively small. The rate of patients in pCR group and non-pCR group was significantly different, which may cause imbalance and affect the robustness of models. Although the data has been augmented by data enhancement, the reduced sample authenticity of the expanded data set may result in unstable model performance. Second, judging pCR by voting on the number of frames may be inappropriate and we will consider improving the algorithm in three dimensions to reduce this error. Third, the model does not use the clinical data of patients, so it is necessary to carry out subsequent optimization of the model.

5. Conclusion

In this study, we provided an automatic segmentation and classification model based on deep learning for predicting pCR after neoadjuvant treatment. DeepInteg achieved better performance in pCR prediction compared with the model based on CT or MRI alone. DeepInteg provided a robust framework to develop disease-specific tools for automatic delineation of ROI and clinical outcome prediction. Moreover, the DeepInteg that has been well trained in the FOWARC trial can readily help clinicians, radiologists and pathologists accurately identify patients with complete response, which may provide valuable reference for wait-and-watch and sphincter-preserving strategies in rectal cancer patients.

A.

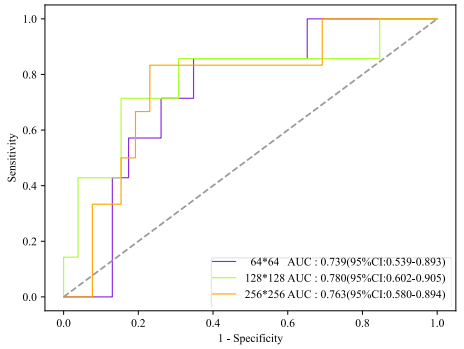

Module		*Accuracy* (95%CI)	*Sensitivity* (95%CI)	*Specificity* (95%CI)
CT	64×64	0.719 (0.542-0.809)	0.592 (0.445-0.720)	0.719 (0.609-0.866)
	128×128	0.781 (0.658-0.858)	0.808 (0.592-0.896)	0.667 (0.527-0.803)
	256×256	0.776 (0.581-0.875)	0.601 (0.352-0.753)	0.762 (0.524-0.836)

B.

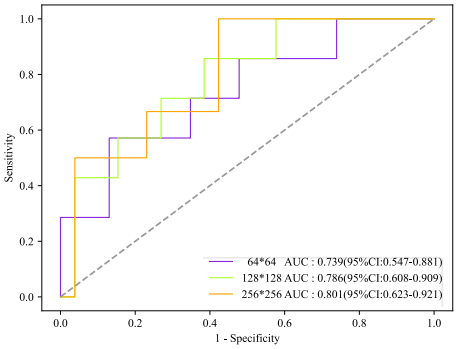

Module		*Accuracy* (95%CI)	*Sensitivity* (95%CI)	*Specificity* (95%CI)
MRI	64×64	0.727 (0.588-0.815)	0.595 (0.592-0.765)	0.760 (0.631-0.852)
	128×128	0.751 (0.558-0.835)	0.484 (0.352-0.731)	0.816 (0.571-0.904)
	256×256	0.752 (0.578-0.847)	0.611 (0.495-0.786)	0.783 (0.661-0.859)

C.

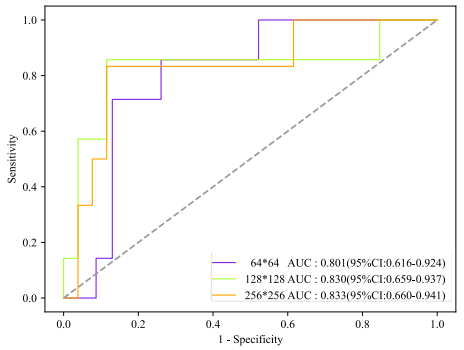

Module		*Accuracy* (95%CI)	*Sensitivity* (95%CI)	*Specificity* (95%CI)
CT&MRI	64×64	0.849 (0.696-0.880)	0.737 (0.664-0.810)	0.854 (0.799-0.918)
	128×128	0.839 (0.739-0.879)	0.799 (0.696-0.904)	0.847 (0.747-0.908)
	256×256	0.826 (0.713-0.894)	0.712 (0.592-0.885)	0.856 (0.748-0.943)

D.

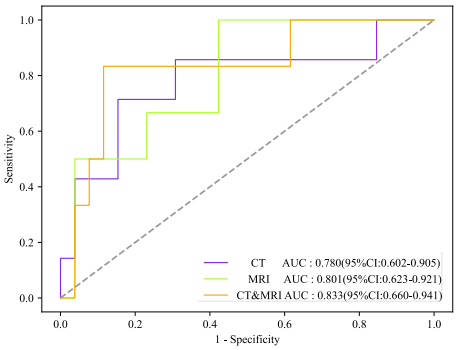

Model	*Accuracy* (95%CI)	*Sensitivity* (95%CI)	*Specificity* (95%CI)
CT	0.781 (0.658-0.858)	0.808 (0.592-0.896)	0.667 (0.527-0.803)
MRI	0.752 (0.578-0.847)	0.611 (0.495-0.786)	0.783 (0.661-0.859)
CT&MRI	0.826 (0.713-0.894)	0.712 (0.592-0.885)	0.856 (0.748-0.943)

(caption on next page)

Fig. 3. Performance of pCR prediction by DeepInteg. The ROC analysis were performed for models based on different sizes of CT image (A), MRI image (B) or integration of CT and MRI image (C). The performance of models based on CT image, MRI image or integration of CT and MRI under the same image size were also compared (D).

Data availability

The clinical information of the patient cohorts used and analyzed in this study are available from Dr. Huichuan Yu on reasonable request.

Code availability

The trained DeepInteg model with the codes for the customed algorithms developed in the current study is available at https://github.com/fzdx123/DeepInteg.

Fundings

This study was supported by the National Natural Science Foundation of China (No. 82272965, HY; No. 81902877, HY), the Natural Science Foundation of Fujian Province (No. 2019J01222, DW), the Natural Science Foundation of Guangdong Province (No. 2022A1515012656, HY), the Science and Technology Program of Guangzhou (No. 202201011004, HY), the Sun Yat-sen University Clinical Research 5010 Program (No. 2018026), the "Five Five" Talent Team Construction Project of the Sixth Affiliated Hospital of Sun Yat-sen University (No. P20150227202010251), the Excellent Talent Training Project of the Sixth Affiliated Hospital of Sun Yat-sen University (No. R2021217202512965), the Scientific Research Project of the Sixth Affiliated Hospital of Sun Yat-sen University (No. 2022JBGS07), the Sixth Affiliated Hospital of Sun Yat-sen University Clinical Research-'1010' Program, the Program of Introducing Talents of Discipline to Universities, and National Key Clinical Discipline (2012).

Declaration of competing interest

The Authors declare no Competing Financial or Non-Financial Interests.

Appendix A. Supplementary data

Supplementary data related to this article can be found at https://doi.org/10.1016/j.heliyon.2023.e13094.

References

[1] D. Killock, Sequential CRT prior to surgery for rectal cancer, Nat. Rev. Clin. Oncol. 18 (2021) 64, https://doi.org/10.1038/s41571-020-00467-9.
[2] P. Sidaway, Neoadjuvant therapy improves pCR rate, Nat. Rev. Clin. Oncol. 17 (2020) 718, https://doi.org/10.1038/s41571-020-00440-6.
[3] D.S. Keller, M. Berho, R.O. Perez, S.D. Wexner, M. Chand, The multidisciplinary management of rectal cancer, Nat. Rev. Gastroenterol. Hepatol. 17 (2020) 414–429, https://doi.org/10.1038/s41575-020-0275-y.
[4] D.R. Byrd, J.D. Brierley, T.P. Baker, D.C. Sullivan, D.M. Gress, Current and future cancer staging after neoadjuvant treatment for solid tumors, CA A Cancer J. Clin. 71 (2021) 140–148, https://doi.org/10.3322/caac.21640.
[5] C.A. Smith, L.A. Kachnic, Evolving treatment paradigm in the treatment of locally advanced rectal cancer, J. Natl. Compr. Cancer Netw. 16 (2018) 909–915, https://doi.org/10.6004/jnccn.2018.7032.
[6] J.J. Smith, P.B. Paty, J. Garcia-Aguilar, Watch and wait in rectal cancer or more wait and see? JAMA Surg 155 (2020) 657–658, https://doi.org/10.1001/jamasurg.2020.0226.
[7] E. Rullier, P. Rouanet, J.J. Tuech, A. Valverde, B. Lelong, M. Rivoire, J.L. Faucheron, et al., Organ preservation for rectal cancer (GRECCAR 2): a prospective, randomised, open-label, multicentre, phase 3 trial, Lancet 390 (2017) 469–479, https://doi.org/10.1016/S0140-6736(17)31056-5.
[8] J.J. Smith, P. Strombom, O.S. Chow, C.S. Roxburgh, P. Lynn, A. Eaton, M. Widmar, et al., Assessment of a watch-and-wait strategy for rectal cancer in patients with a complete response after neoadjuvant therapy, JAMA Oncol. 5 (2019), e185896, https://doi.org/10.1001/jamaoncol.2018.5896.
[9] J.J. Smith, P.B. Paty, J. Garcia-Aguilar, Watch and wait in rectal cancer or more wait and see? JAMA Surgery 155 (2020) 657–658, https://doi.org/10.1001/jamasurg.2020.0226.
[10] G. Emons, N. Auslander, P. Jo, J. Kitz, A. Azizian, Y. Hu, C.F. Hess, et al., Gene-expression profiles of pretreatment biopsies predict complete response of rectal cancer patients to preoperative chemoradiotherapy, Br. J. Cancer (2022), https://doi.org/10.1038/s41416-022-01842-2.
[11] L. Feng, Z. Liu, C. Li, Z. Li, X. Lou, L. Shao, Y. Wang, et al., Development and validation of a radiopathomics model to predict pathological complete response to neoadjuvant chemoradiotherapy in locally advanced rectal cancer: a multicentre observational study, Lancet Digit Health 4 (2022) e8–e17, https://doi.org/10.1016/S2589-7500(21)00215-6.
[12] V.S. Jayaprakasam, V. Paroder, P. Gibbs, R. Bajwa, N. Gangai, R.E. Sosa, I. Petkovska, et al., MRI radiomics features of mesorectal fat can predict response to neoadjuvant chemoradiation therapy and tumor recurrence in patients with locally advanced rectal cancer, Eur. Radiol. 32 (2022) 971–980, https://doi.org/10.1007/s00330-021-08144-w.
[13] Z. Zhuang, Z. Liu, J. Li, X. Wang, P. Xie, F. Xiong, J. Hu, et al., Radiomic signature of the FOWARC trial predicts pathological response to neoadjuvant treatment in rectal cancer, J. Transl. Med. 19 (2021) 256.
[14] D.L. Ren, J. Li, H.C. Yu, S.Y. Peng, W.D. Lin, X.L. Wang, R.A. Ghoorun, et al., Nomograms for predicting pathological response to neoadjuvant treatments in patients with rectal cancer, World J. Gastroenterol. 25 (2019) 118–137.
[15] W. Buchberger, W. Oberaigner, C. Kremser, K. Gautsch, U. Siebert, Non-mass enhancement in breast MRI: characterization with BI-RADS descriptors and ADC values, SciMedicine J. 3 (2021) 77–87, https://doi.org/10.28991/SciMedJ-2021-0302-1.

[16] K. Bera, N. Braman, A. Gupta, V. Velcheti, A. Madabhushi, Predicting cancer outcomes with radiomics and artificial intelligence in radiology, Nat. Rev. Clin. Oncol. 19 (2022) 132–146, https://doi.org/10.1038/s41571-021-00560-7.
[17] O. Elemento, C. Leslie, J. Lundin, G. Tourassi, Artificial intelligence in cancer research, diagnosis and therapy, Nat. Rev. Cancer 21 (2021) 747–752, https://doi.org/10.1038/s41568-021-00399-1.
[18] P. Rajpurkar, E. Chen, O. Banerjee, E.J. Topol, AI in health and medicine, Nat. Med. 28 (2022) 31–38, https://doi.org/10.1038/s41591-021-01614-0.
[19] M. Bakhsheshi, M. Ho, L. Keenliside, T.-Y. Lee, Non-invasive monitoring of brain temperature during rapid selective brain cooling by zero-heat-flux thermometry, Emerging Sci. J. 3 (2019) 1, https://doi.org/10.28991/esj-2019-01163.
[20] M. Hou, L. Zhou, J. Sun, Deep-learning-based 3D super-resolution MRI radiomics model: superior predictive performance in preoperative T-staging of rectal cancer, Eur. Radiol. (2022), https://doi.org/10.1007/s00330-022-08952-8.
[21] X. Liu, D. Zhang, Z. Liu, Z. Li, P. Xie, K. Sun, W. Wei, et al., Deep learning radiomics-based prediction of distant metastasis in patients with locally advanced rectal cancer after neoadjuvant chemoradiotherapy: a multicentre study, EBioMedicine 69 (2021), 103442, https://doi.org/10.1016/j.ebiom.2021.103442.
[22] H.M. Thompson, J.K. Kim, R.M. Jimenez-Rodriguez, J. Garcia-Aguilar, H. Veeraraghavan, Deep learning-based model for identifying tumor in endoscopic images from patients with locally advanced rectal cancer treated with total neoadjuvant therapy, Dis. Colon Rectum (2022), https://doi.org/10.1097/DCR.0000000000002295.
[23] X.Y. Zhang, L. Wang, H.T. Zhu, Z.W. Li, M. Ye, X.T. Li, Y.J. Shi, et al., Predicting rectal cancer response to neoadjuvant chemoradiotherapy using deep learning of diffusion kurtosis MRI, Radiology 296 (2020) 56–64, https://doi.org/10.1148/radiol.2020190936.
[24] Y. Deng, P. Chi, P. Lan, L. Wang, W. Chen, L. Cui, D. Chen, et al., Modified FOLFOX6 with or without radiation versus fluorouracil and leucovorin with radiation in neoadjuvant treatment of locally advanced rectal cancer: initial results of the Chinese FOWARC multicenter, open-label, randomized three-arm phase III trial, J. Clin. Oncol. 34 (2016) 3300–3307, https://doi.org/10.1200/JCO.2016.66.6198.
[25] Y. Deng, P. Chi, P. Lan, L. Wang, W. Chen, L. Cui, D. Chen, et al., Neoadjuvant modified FOLFOX6 with or without radiation versus fluorouracil plus radiation for locally advanced rectal cancer: final results of the Chinese FOWARC trial, J. Clin. Oncol. 37 (2019) 3223–3233, https://doi.org/10.1200/JCO.18.02309.
[26] D. Shen, X. Wang, H. Wang, G. Xu, Y. Xie, Z. Zhuang, Z. Huang, et al., Current surveillance after treatment is not sufficient for patients with rectal cancer with negative baseline CEA, J. Natl. Compr. Cancer Netw. (2022) 1–10, https://doi.org/10.6004/jnccn.2021.7101.
[27] Y. Xie, J. Lin, X. Wang, P. Wang, Z. Zhuang, Q. Zou, D. Cai, et al., The Addition of Preoperative Radiation Is Insufficient for Lateral Pelvic Control in a Subgroup of Patients with Low Locally Advanced Rectal Cancer: A Post-Hoc Study of a Randomized Controlled Trial. Diseases of the Colon and Rectum, 2021.
[28] J. Li, Y. Xie, Z. Huang, D. Shen, Z. Zhuang, M. Zhu, Y. Huang, et al., Current treatment and surveillance modalities are not sufficient for advanced stage III colon cancer: result from a multicenter cohort analysis, Cancer Med. 10 (2021) 8924–8933.
[29] A. Trakarnsanga, M. Gönen, J. Shia, G.M. Nash, L.K. Temple, J.G. Guillem, P.B. Paty, et al., Comparison of tumor regression grade systems for locally advanced rectal cancer after multimodality treatment, JNCI (J. Natl. Cancer Inst.) 106 (2014) dju248, https://doi.org/10.1093/jnci/dju248.
[30] I. Kandel, M. Castelli, L. Manzoni, Brightness as an augmentation technique for image classification, Emerging Sci. J. 6 (2022) 881–892, https://doi.org/10.28991/ESJ-2022-06-04-015.
[31] Z. Gu, J. Cheng, H. Fu, K. Zhou, H. Hao, Y. Zhao, T. Zhang, et al., CE-net: context encoder network for 2D medical image segmentation, IEEE Trans. Med. Imag. 38 (2019) 2281–2292, https://doi.org/10.1109/TMI.2019.2903562.
[32] O. Ronneberger, P. Fischer, T. Brox, U-net: convolutional networks for biomedical image segmentation, in: N. Navab, J. Hornegger, W.M. Wells, A.F. Frangi (Eds.), Medical Image Computing and Computer-Assisted Intervention – MICCAI 2015; 2015 2015//, Springer International Publishing, Cham, 2015, pp. 234–241.
[33] K. Kim, S. Kim, K. Han, H. Bae, J. Shin, J.S. Lim, Diagnostic performance of deep learning-based lesion detection algorithm in CT for detecting hepatic metastasis from colorectal cancer, Korean J. Radiol. 22 (2021) 912–921, https://doi.org/10.3348/kjr.2020.0447.
[34] J. Fu, X. Zhong, N. Li, R. Van Dams, J. Lewis, K. Sung, A.C. Raldow, et al., Deep learning-based radiomic features for improving neoadjuvant chemoradiation response prediction in locally advanced rectal cancer, Phys. Med. Biol. 65 (2020), 075001, https://doi.org/10.1088/1361-6560/ab7970.
[35] J.C. Kim, T.W. Kim, J.H. Kim, C.S. Yu, H.C. Kim, H.M. Chang, M.H. Ryu, et al., Preoperative concurrent radiotherapy with capecitabine before total mesorectal excision in locally advanced rectal cancer, Int. J. Radiat. Oncol. Biol. Phys. 63 (2005) 346–353, https://doi.org/10.1016/j.ijrobp.2005.02.046.